Electronic Supplementary Information for

Unlocking the Action Mechanisms of Molecular Nonlinear Optical Absorption for Optical Conjugated Polymers under Aggregation States

Jin Huang,[a,b] Dong Zheng,[a,c] Bang'an Peng,[a] Menghao Kong,[b] Yixiao Hang,[b] Jing Ma*[a,c] and Xudong Jia*[a]

[a] *State Key Laboratory of Coordination Chemistry, Department of Polymer Science & Engineering, Nanjing University, Nanjing 210023, PR China.*

E-mail: jiaxd@nju.edu.cn

[b] *Institute of Advanced Synthesis, School of Chemistry and Molecular Engineering, Jiangsu National Synergetic Innovation Center for Advanced Materials, Nanjing Tech University, Nanjing 211816, China.*

[c] *Key Laboratory of Mesoscopic Chemistry of MOE, School of Chemistry & Chemical Engineering, Nanjing University, Nanjing 210023, PR China*

E-mail: majing@nju.edu.cn

Contents

1. Materials

tetrakis(triphenylphosphine)palladium(0) (99.5%), 3,6-dibromo-9*H*-carbazole (99%), 1-bromohexane (99%), anhydrous potassium carbonate (98%), tetrabutylammonium bromide (98%), bromobenzene (98%) were purchased from Adamas. 2,5-dibromo-3,4-dinitrothiophene (98%) (M2) was used as received from Puyang Huicheng Electronic Material Co. Ltd. 2,2'-(9,9-dioctyl-9*H*-fluorene-2,7-diyl)bis(1,3,2-dioxaborinane) (M1) (99%) was purchased from Derthon Optoelectronic Materials Science Technology Co LTD (Shenzhen, China). All the reactions were carried out under nitrogen atmosphere. All organic solvents were purchased from commercial sources and were carefully dried and distilled prior to use.

2. Syntheses and Characterization of Compounds

2.1 Synthesis of 3,6-dibromo-9-hexyl-9*H*-carbazole

Under argon atmosphere, 3,6-dibromo-9*H*-carbazole (13.00 g, 0.04 mol), powdered anhydrous potassium carbonate (11.06 g, 0.08 mol), anhydrous acetonitrile (160 mL) and 1,10-dibromodecane (6.60 g, 0.04 mol) were placed in a reaction flask fitted with a condenser. The reaction was refluxed at 95 °C for 36 h and the argon atmosphere was maintained throughout the reaction. After cooling to room temperature, the precipitation was filtered, and the solvent was removed under reduced pressure to get crude product. The crude product was recrystallized from petroleum ether to give white crystals (8.67 g, Yield 53%). ^{1}H NMR (500 MHz, $CDCl_3$, δ): 8.09 (s, 2 H, Ar–H), 7.51 (d, *J* =8.9 Hz, 2 H, Ar–H), 7.24 (d, *J* =8.9 Hz, 2 H, Ar–H), 4.18 (t, *J* =7.6 Hz, 2 H, –NCH_2), 1.79(m, 2 H), 1.28 (m, 6 H), 0.83 (t, *J*

=9.0 Hz, 3 H, –CH_3). ^{13}C NMR (500 MHz, $CDCl_3$, δ): 139.1, 129.1, 123.4, 123.2, 112.1, 110.6, 43.4, 31.3, 28.9, 26.7, 22.5, 13.9. Anal. Calcd. For $C_{22}H_{26}Br_3N$: C, 52.84; H, 4.68; N, 3.42. Found: C, 52.67; H, 4.82; N, 3.49.

2.2 Calculation of the actual composition in the main chain of polymers

The actual proportion of donor unit (the copolymer unit from M1 and M3) and acceptor unit (the copolymer unit from M1 and M2) in D1–D2–D1–A-type OCPs could be measured by ^{1}H NMR. The characteristic peak **a** at about 4.40 ppm belongs to -NCH_2, the characteristic peak **b** at about 1.60~0.80 ppm is attributed to –CH_2 for D-A-type OCPs (see Figure S6~S10). Therefore, the proportion of donor unit and acceptor unit could be calculated by the integration area ratio of **a** and **b** peak . The **x** and **y** values were calculated according to the given equation:

$$\mathbf{X+Y=1,} \qquad \mathbf{I_b/I_a = (4X+2X+4Y)/2X}$$

The calculation results were listed in the following table S1.

"x" refer to the proportion of donor unit in the main chain of polymers, "y" refer to the proportion of acceptor unit in the main chain of D1–D2–D1–A-type OCPs. "I_b/I_a" is the integration area ratio of **b** and **a** peak in the ^{1}H NMR spectra of $P_{0.05}$, $P_{0.1}$, $P_{0.2}$, $P_{0.3}$, $P_{0.4}$.

Table S1. The actual composition in the main chain of polymers

Polymer	The integration area ratio of **a** and **b** peak ($\mathbf{I_b/I_a}$)	x and y value
$P_{0.05}$	3.17	x = 0.92, y = 0.08
$P_{0.1}$	3.44	x = 0.82, y = 0.18
$P_{0.2}$	3.67	x = 0.75, y = 0.25
$P_{0.3}$	4.28	x = 0.61, y = 0.39
$P_{0.4}$	5.17	x = 0.48, y = 0.52

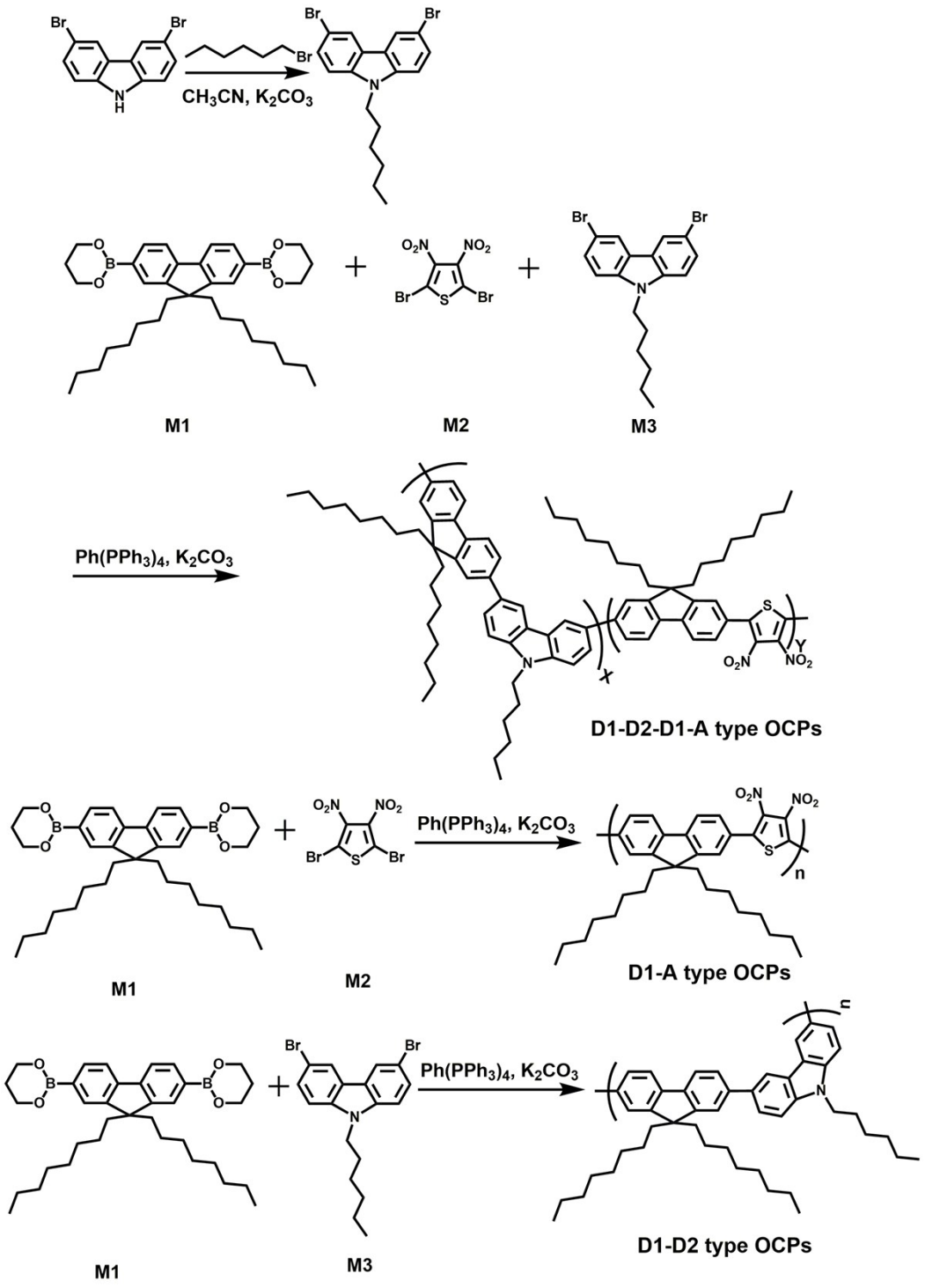

Figure S1. Synthesis of D1–D2-type, D1–A-type and D1–D2–D1–A-type OCPs

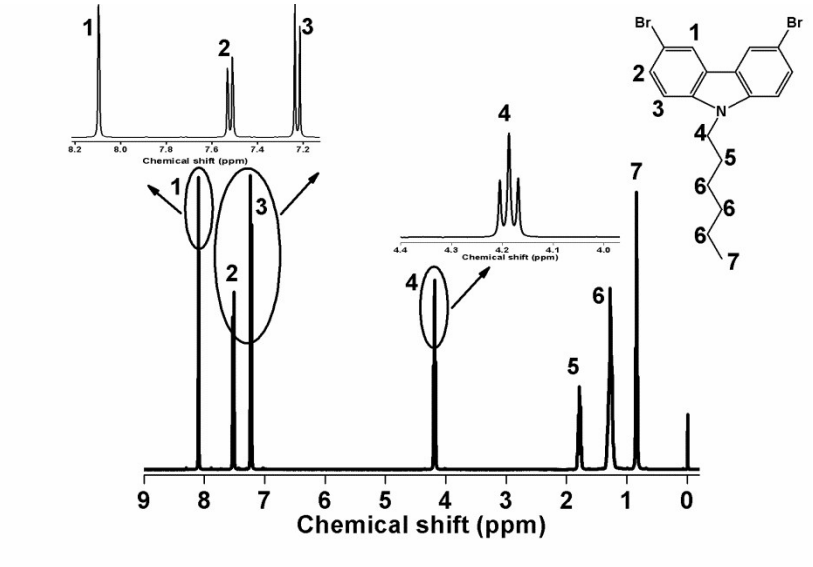

Figure S2. The ^{1}H NMR spectra of 3,6-dibromo-9-hexyl-9*H*-carbazole. (500 MHz, $CDCl_3$)

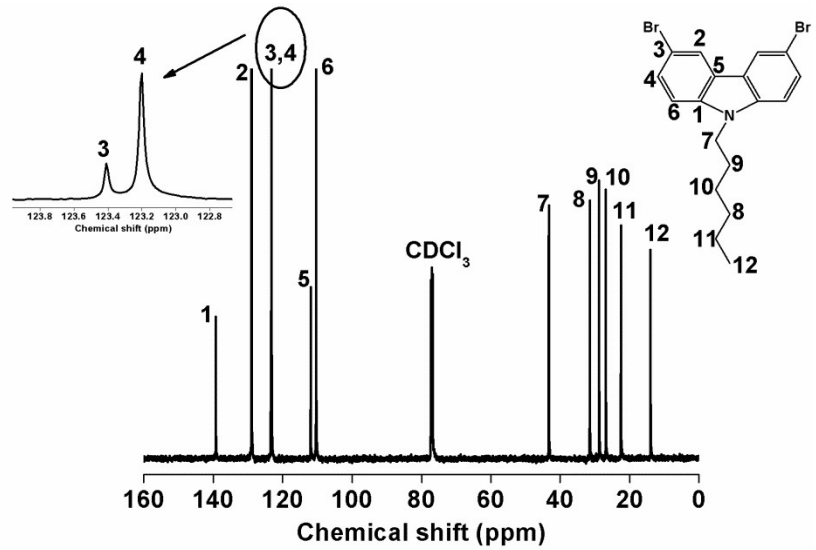

Figure S3. The ^{13}C NMR spectra of 3,6-dibromo-9-hexyl-9*H*-carbazole. (500 MHz, $CDCl_3$)

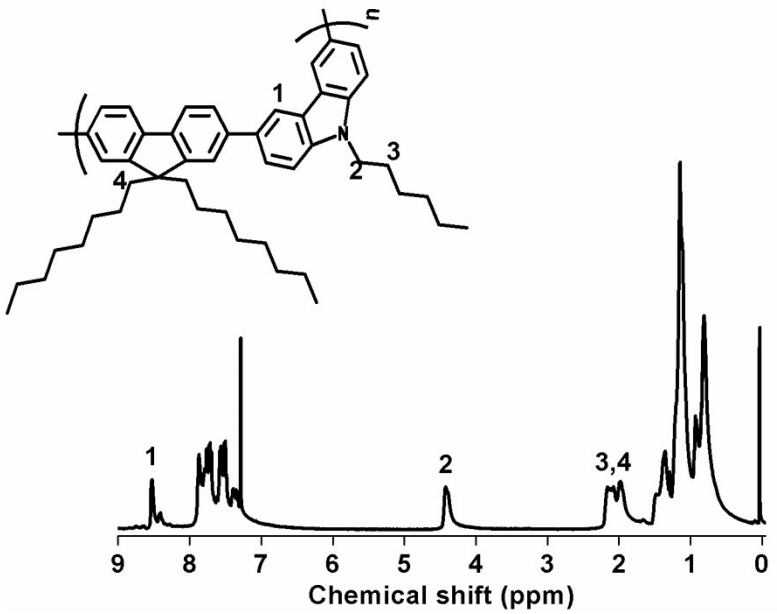

Figure S4. The ^{1}H NMR spectra of P_0 (D1-D2 type OCPs). (500 MHz, $CDCl_3$)

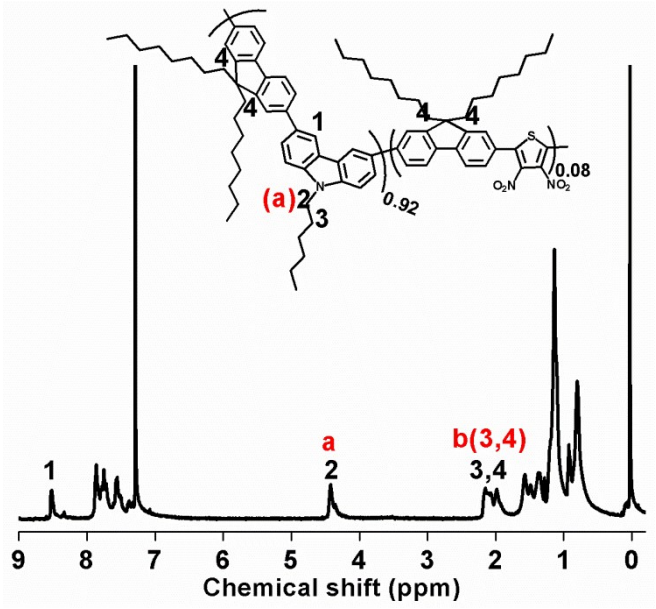

Figure S5. The ^{1}H NMR spectra of $P_{0.05}$ (D1–D2–D1–A-type OCPs). (500 MHz, $CDCl_3$)

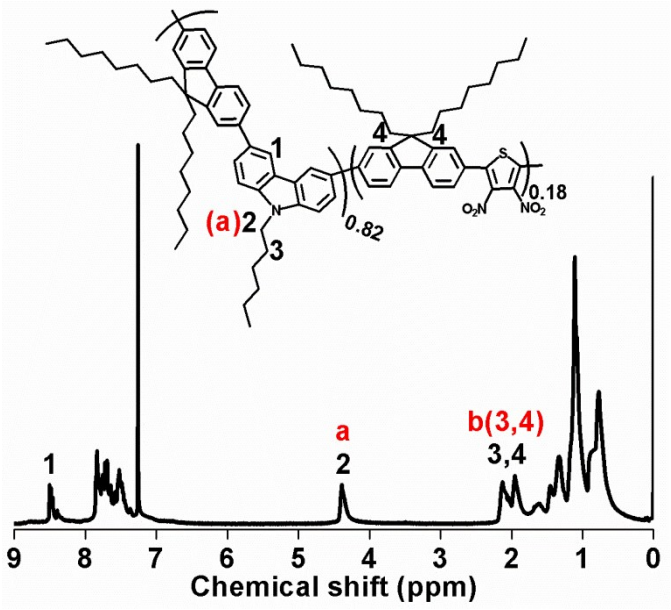

Figure S6. The ^{1}H NMR spectra of $P_{0.1}$ (D1–D2–D1–A-type OCPs). (500 MHz, $CDCl_3$)

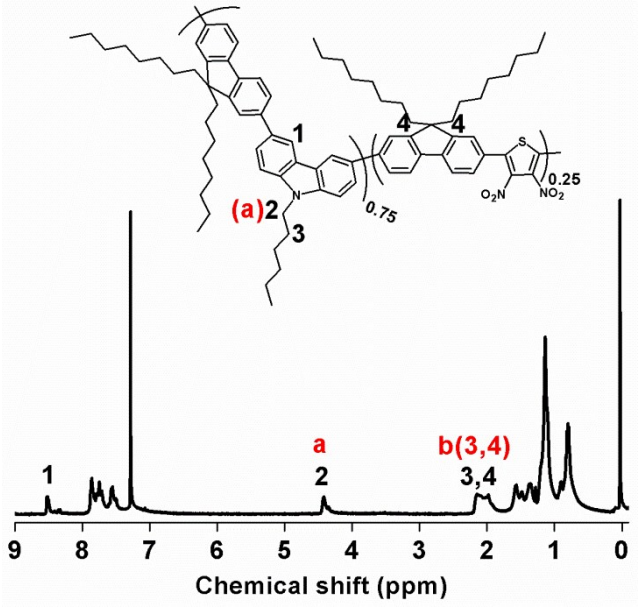

Figure S7. The ^{1}H NMR spectra of $P_{0.2}$ (D1–D2–D1–A-type OCPs). (500 MHz, $CDCl_3$)

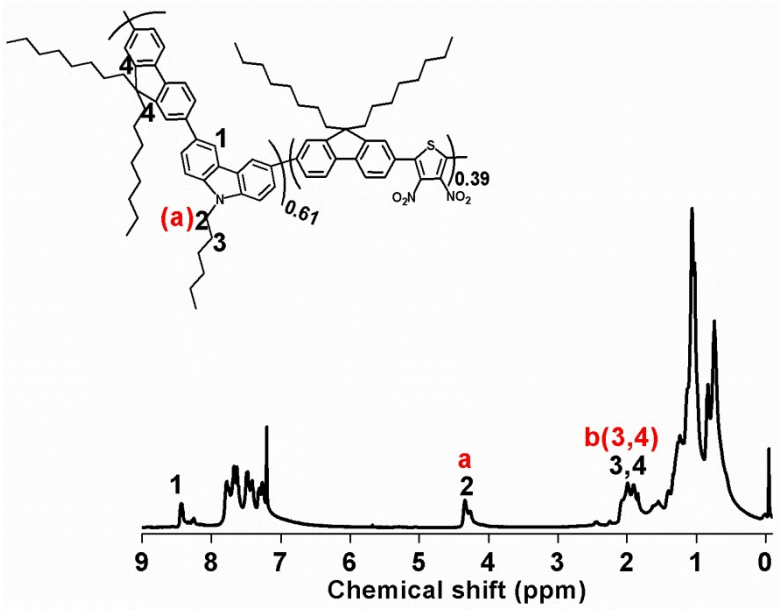

Figure S8. The ^{1}H NMR spectra of $P_{0.3}$ (D1–D2–D1–A-type OCPs). (500 MHz, $CDCl_3$)

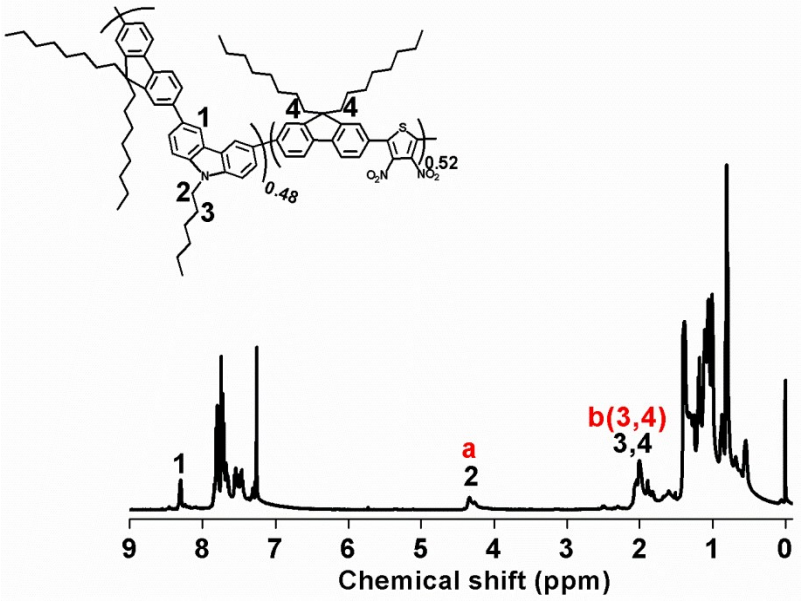

Figure S9. The ^{1}H NMR spectra of $P_{0.4}$ (D1–D2–D1–A-type OCPs). (500 MHz, $CDCl_3$)

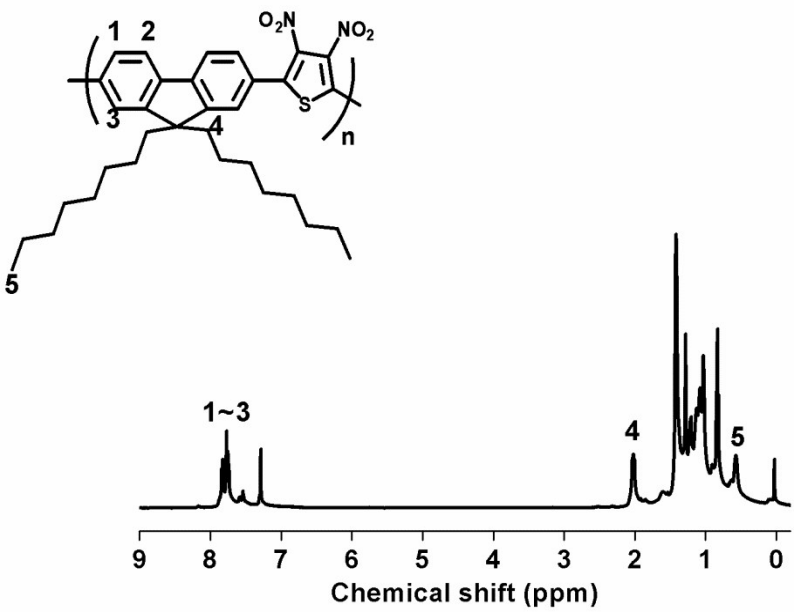

Figure S10. The ^{1}H NMR spectra of P_1 (D1-A type OCPs). (500 MHz, $CDCl_3$)

3. Supplementary Figures of Compounds.

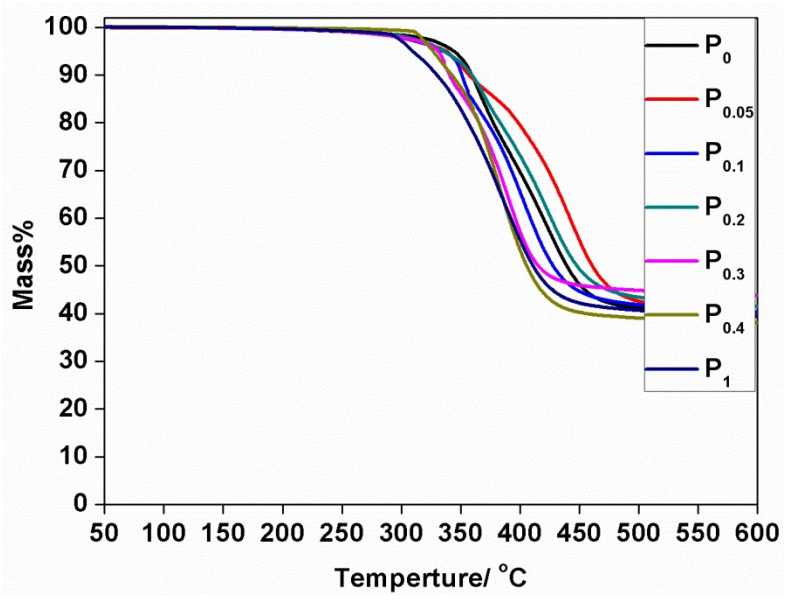

Figure S11. TGA thermograms of the OCPs at a ramp rate of 10 °C/min in nitrogen flow.

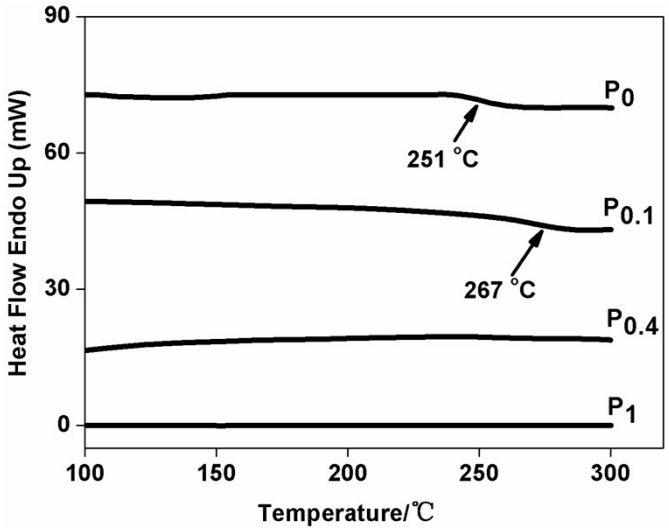

Figure S12. DSC curves of P_0, $P_{0.1}$, $P_{0.4}$, P_1 at a ramp rate of 10 °C/min in nitrogen flow

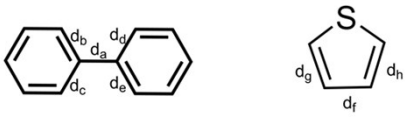

$$d_1 = 0.25(d_b + d_c + d_d + d_e)$$

$$\delta_1 = \frac{d_a - d_1}{(d_a + d_1)/2}$$

$$d_2 = 0.5(d_g + d_h)$$

$$\delta_2 = \frac{d_f - d_2}{(d_f + d_2)/2}$$

Figure S13. For the intermolecular BLA parameter is defined as δ_1 where d_m (m=b-f) denotes the length of each CC bond in the ring. Similarly, BLA parameter in thiophene unit is defined as δ_2. The BLA parameters reflect the degrees of conjugation of the conjugated ring, because they provide a direct measurement of differences in length between single and double CC bonds that involved.

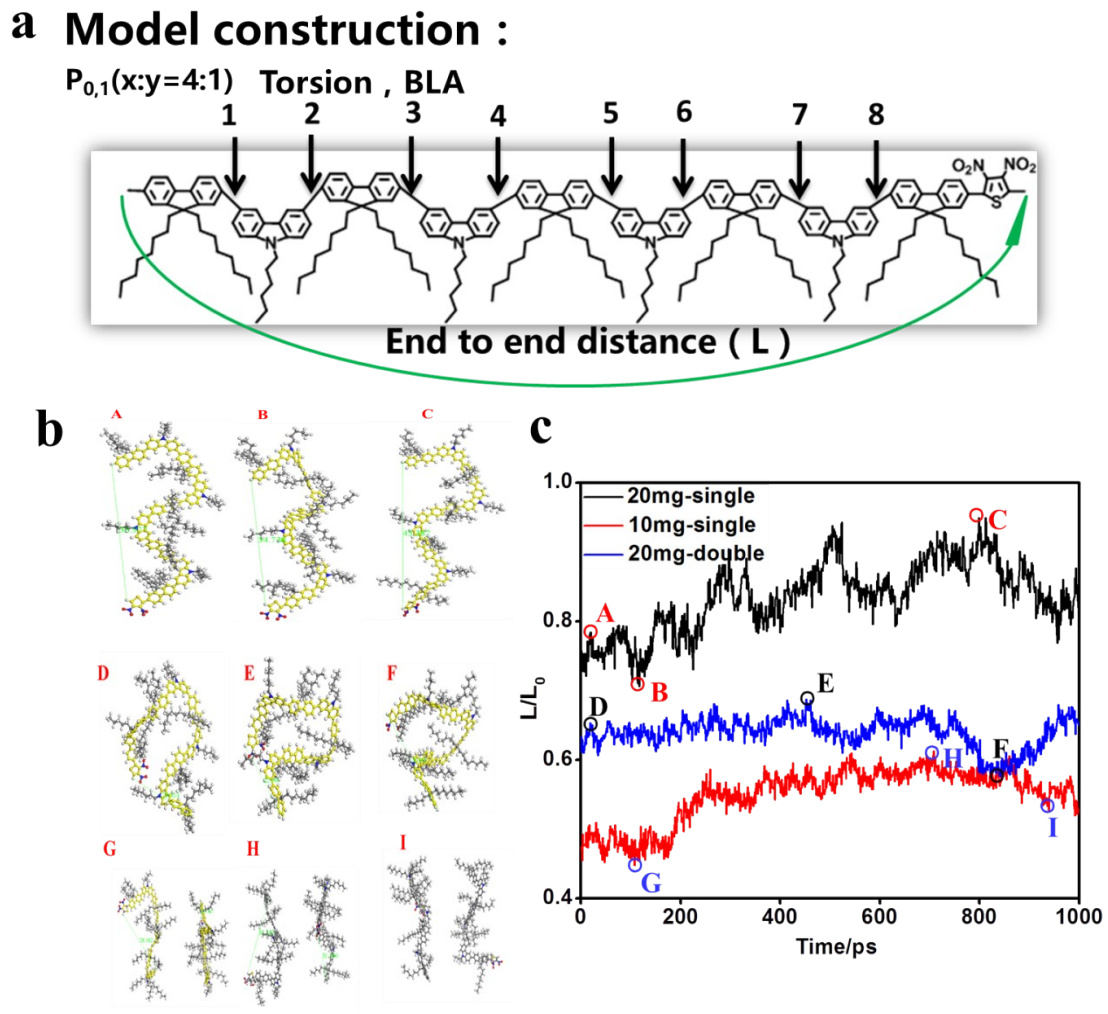

Figure S14. Illustrations of (a) simulation model of $P_{0.1}$ in THF solutions with the definition of the end to end distance L and the numeric labels (1-8) of the eight inter-unit C-C linkage for evaluation of torsion angles (D) and BLA (δ) and (b) slected snapshots (A-I) with some typical conformations along (c) molecular dynamics trajectories with different concentrations (10 mg/ml and 20 mg/ml) and different intial settings with (double) and without (single) consideration of inter-chain interactions in the simulation box with periodic boundary conditions.

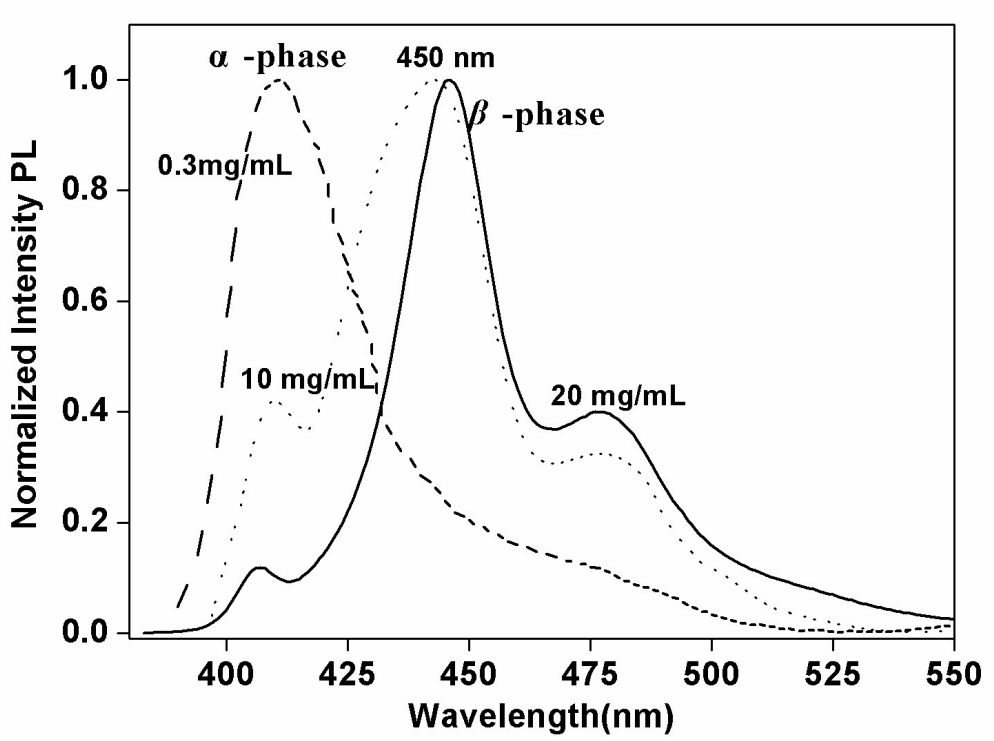

Figure S15. The PL spectra of $P_{0.1}$ under different concentrations (0.3 mg/mL, 10 mg/mL, 20mg/mL)

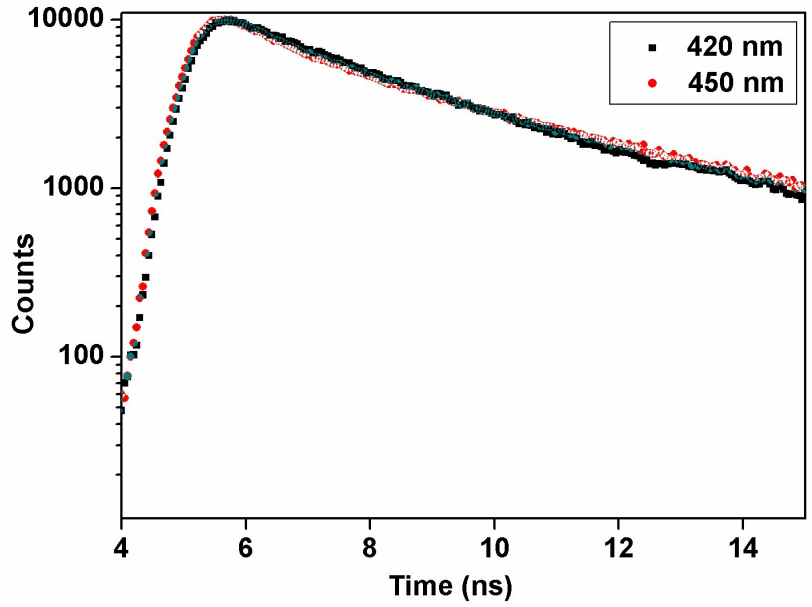

Figure S16. Time-resolved fluorescence decay curves of $P_{0.1}$ dilute solution (0.3 mg/mL) at 420 nm and 450 nm

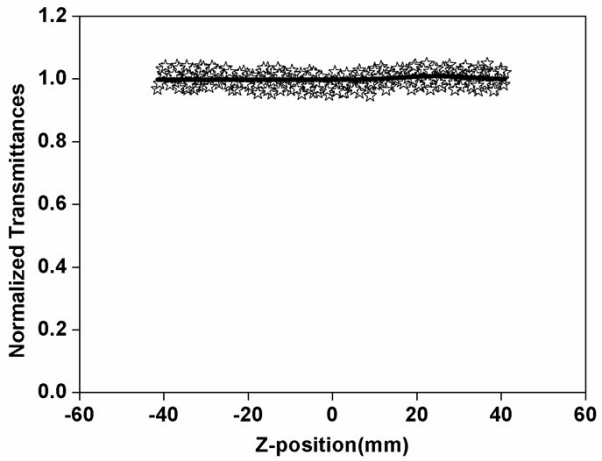

Figure S17. Open-aperture Z-scan curves of $P_{0.1}$ in 0.3 mg/mL THF solution

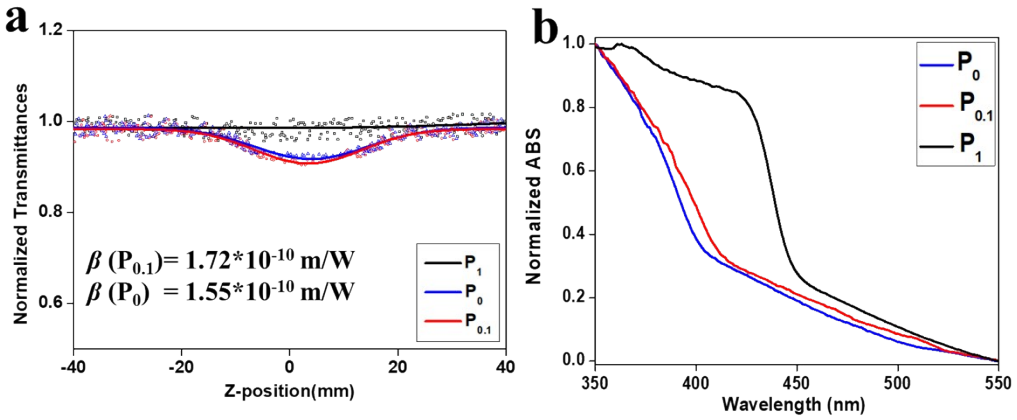

Figure S18. (a) Open-aperture Z-scan curves of pure P_0, $P_{0.1}$ and P_1 film at 532 nm with 4-ns pulses; (b) Normalized UV-vis spectra of pure P_0, $P_{0.1}$ and P_1 films. The solid films were obtained by spin-coating 10 mg/mL polymer solution in THF onto quartz glass slide with a spinning rate of 500 rpm.

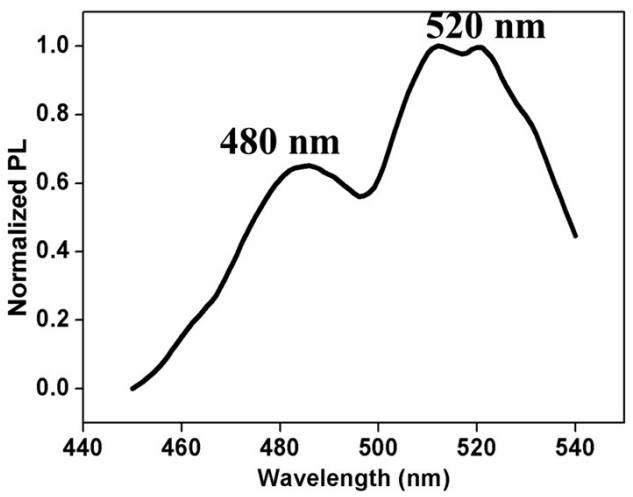

Figure S19. Normalized PL spectrum of pure $P_{0.1}$ film.

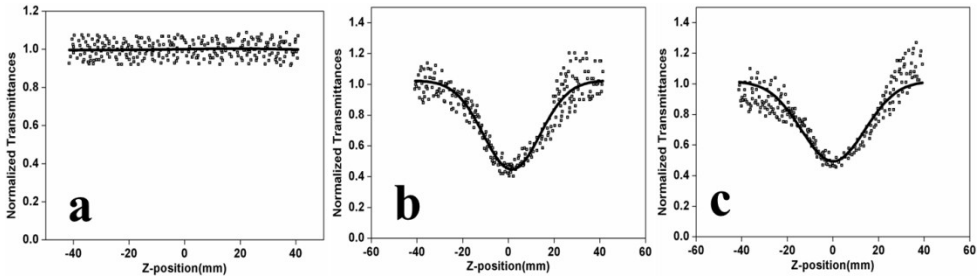

Figure S20. Open-aperture Z-scan curves of OCPs/PMMA composite films doped with a) 0%, b) 0.03% and c) 0.08% mass fraction

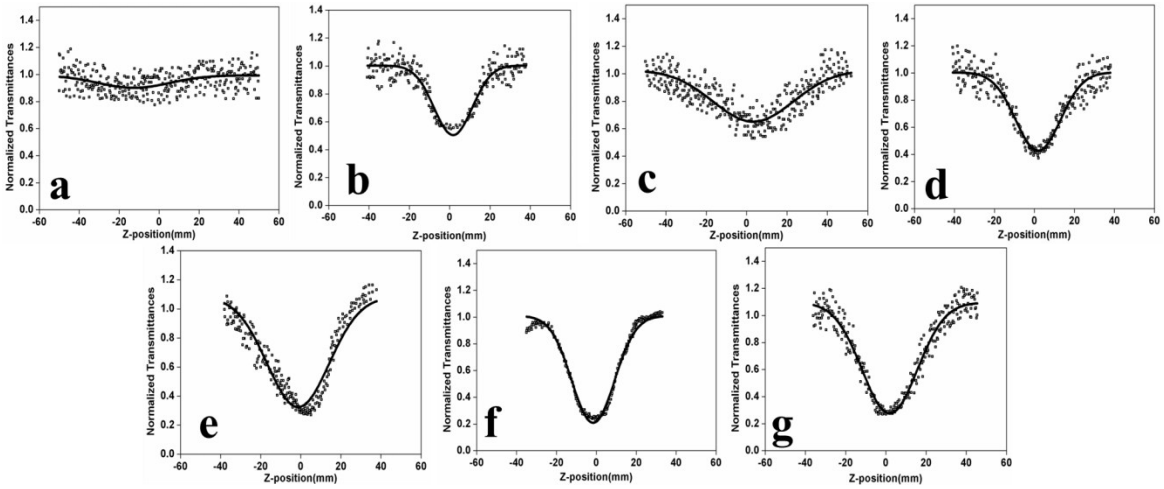

Figure S21. Open-aperture Z-scan curves of OCPs/PS composite films doped with a) 0%, b) 0.01%, c) 0.03%, d) 0.05%, e) 0.08%, f) 0.1%, g) 0.3% mass fraction

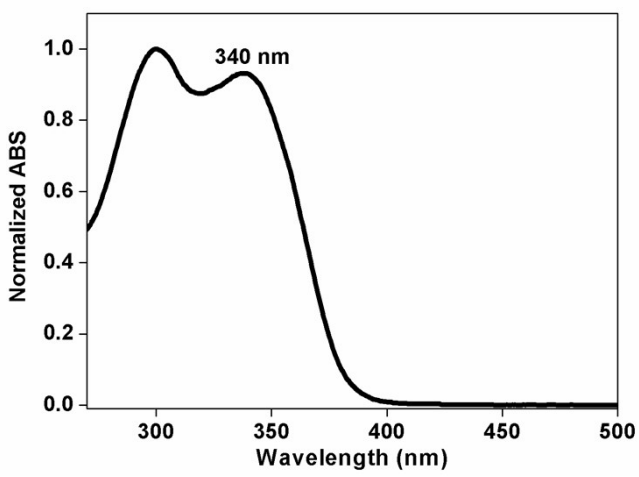

Figure S22. The normalized ABS spectra of PMMA pure solid film

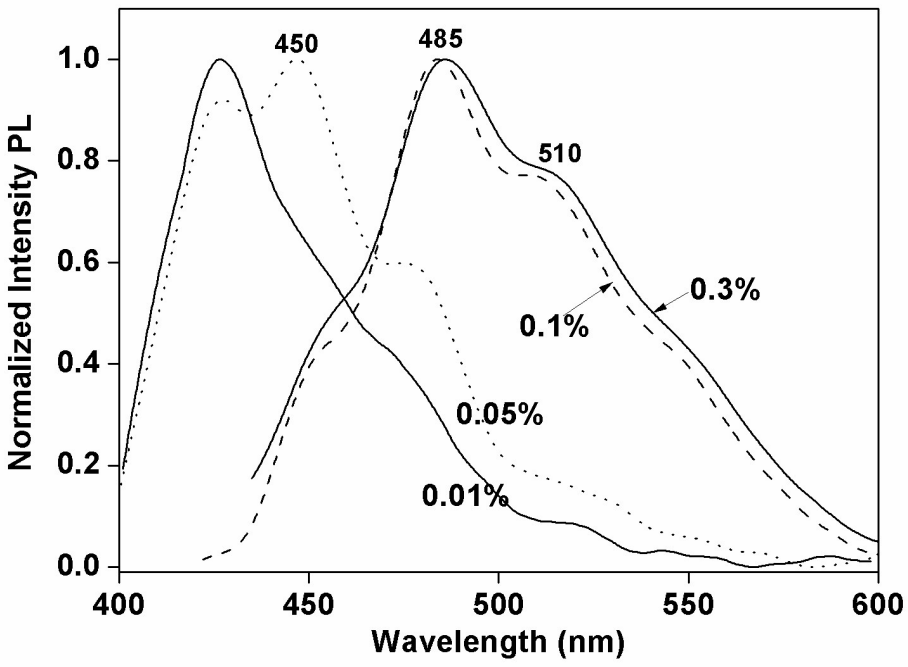

Figure S23. The normalized PL spectra of OCPs/PS composite films doped with 0.01%, 0.05%, 0.1% and 0.3% mass fraction

Table S2. The Nonlinear Absorption Coefficient of the OCPs in 20 mg/mL THF Solution

Polymer	Nonlinear Absorption Coefficient (10^{-10} m/W)

P_0 (D1-D2 type)	3.02
$P_{0.05}$	5.51
$P_{0.1}$	5.96
$P_{0.2}$	5.39
$P_{0.3}$	5.17
$P_{0.4}$	5.03
P_1 (D1-A type)	4.75

Table S3. Details of various simulation models used in NVT MD simulations with PCFF at 298 K.

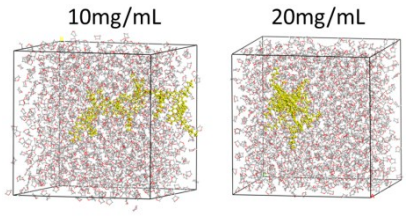

substance	N_{solute}	$N_{solvent}$	C (mg/mL)	ρ (g/cm^3)	PBC cell/Å
$P_{0.1}$@THF	1	3839	10	0.889	81×81×81
$P_{0.1}$@THF	1	1919	20	0.889	60×60×60

Table S4. The fluorescence lifetime and QY of different concentrations and their ratio

Concentration (mg/mL)	τ_1 (ns)	A_1 (%)	τ_2 (ns)	A2 (%)	τ_a (ns)	Φ_F (%)
0.3	2.57	100	/	/	/	/
5	1.96	94.36	4.72	5.64	2.12	3.32

10	1.85	90.17	3.51	9.83	2.01	4.19
20	1.67	87.92	3.38	12.08	1.88	6.05

The fluorescence lifetime for the emission wavelength at 450 nm, average lifetime τ calculated by the equation $\tau_a = A1\tau_1 + A2\tau_2$, A1 and A2 is the percentage of fluorescence lifetime τ_1 and τ_2 respectively. Φ_F = fluorescence quantum yield determined using a calibrated integrating sphere.

Table S5. The QY of the polymeric solid films

Polymer	Φ_F (%)
P_0	2.17
$P_{0.05}$	1.93
$P_{0.1}$	1.65
$P_{0.2}$	1.21
$P_{0.3}$	/
$P_{0.4}$	/
P_1	/

Φ_F = fluorescence quantum yield determined using a calibrated integrating sphere (Edinburgh Instruments FLS980).

Table S6. The fluorescence lifetime and QY of $P_{0.1}$/PMMA composite films

Doped mass fraction (%)	τ_1 (ns)	A_1 (%)	τ_2 (ns)	A2 (%)	τ_a （ns）	Φ_F (%)
0.01	1.24	4.56	60.50	39.50	2.55	4.92
0.03	1.21	4.09	60.32	39.68	2.35	5.88
0.05	1.02	3.67	66.86	33.14	1.90	7.12
0.08	0.96	3.58	73.60	26.40	1.65	8.36
0.3	0.97	3.44	67.71	32.29	1.77	5.07